AIP | Review of Scientific Instruments

Development of a tunable Fabry-Perot etalon-based near-infrared interference spectrometer for measurement of the HeI 23S-23P spectral line shape in magnetically confined torus plasmas

S. Ogane, T. Shikama, H. Zushi, and M. Hasuo

Citation: Review of Scientific Instruments **86**, 103507 (2015); doi: 10.1063/1.4931804
View online: http://dx.doi.org/10.1063/1.4931804
View Table of Contents: http://scitation.aip.org/content/aip/journal/rsi/86/10?ver=pdfcov
Published by the AIP Publishing

REVIEW OF SCIENTIFIC INSTRUMENTS **86**, 103507 (2015)

Development of a tunable Fabry-Perot etalon-based near-infrared interference spectrometer for measurement of the HeI 2^3S-2^3P spectral line shape in magnetically confined torus plasmas

S. Ogane,[1] T. Shikama,[1,a)] H. Zushi,[2] and M. Hasuo[1]
[1]*Department of Mechanical Engineering and Science, Graduate School of Engineering, Kyoto University, Kyoto 615-8540, Japan*
[2]*Research Institute for Applied Mechanics, Kyushu University, Fukuoka 816-8580, Japan*

(Received 27 April 2015; accepted 14 September 2015; published online 14 October 2015)

In magnetically confined torus plasmas, the local emission intensity, temperature, and flow velocity of atoms in the inboard and outboard scrape-off layers can be separately measured by a passive emission spectroscopy assisted by observation of the Zeeman splitting in their spectral line shape. To utilize this technique, a near-infrared interference spectrometer optimized for the observation of the helium 2^3S–2^3P transition spectral line (wavelength 1083 nm) has been developed. The applicability of the technique to actual torus devices is elucidated by calculating the spectral line shapes expected to be observed in LHD and QUEST (Q-shu University Experiment with Steady State Spherical Tokamak). In addition, the Zeeman effect on the spectral line shape is measured using a glow-discharge tube installed in a superconducting magnet. © *2015 AIP Publishing LLC.* [http://dx.doi.org/10.1063/1.4931804]

I. INTRODUCTION

In the scrape-off layer (SOL) of magnetically confined torus plasmas, a complex ion flow structure, which affects particle transport toward the divertor plate and impurity screening from the core plasma, is generated.[1,2] The ion flow is partly driven by atoms through a pressure gradient induced by ionization and recombination[3,4] and partly dissipated through friction mediated by charge-exchange.[5] The former can be affected by the spatial distributions of the ionizing and recombining fluxes and the enhancement of the ionization by radiation reabsorption;[6,7] the magnitudes of these effects are functions of the atomic density, temperature, and flow velocity. Meanwhile the latter can be affected by the atomic density via the rate coefficient of the charge-exchange reaction. In addition, momentum transferred to atoms can change their transport[5] and thus the spatial distribution of the ionizing flux.

For spatially resolved diagnostics of the atomic density, temperature, and flow velocity in the SOL, a passive emission spectroscopic technique that utilizes magnetic field effects on the spectral line shapes of atoms has been developed.[5,8–11] This technique determines the location of the spectral line emission from the observed magnitude of the Zeeman splitting and the known spatial distribution of the magnetic field. In particular, by adopting a radial viewing chord near the midplane, superposed emissions emanating from the inboard and outboard SOLs can be separated by using the difference in their spectral line shapes. Local values of the emission intensity and the Doppler broadening and shift can then be evaluated from the separated spectral line shapes.[5,9–11]

The application of this technique requires a larger Zeeman splitting than spectral line broadening. The observation of a spectral line with a relatively long wavelength is thus advantageous, since the magnitude of the Zeeman splitting is approximately proportional to the square of the wavelength, while that of the Doppler broadening is proportional to it. In fusion-related plasmas, one should also consider the effect of black-body radiation emanating from the plasma facing components, whose surface temperature can increase to nearly 1000 K and locally exceed 1000 K.[12,13] The effect of the radiation therefore can be large in the mid- and far-infrared regions, and the dynamic range of a detector in the measurement of an atomic spectral line would be decreased. To reduce the effect of the black-body radiation and to utilize the wavelength proportionality, we apply the present technique to a spectral line in the near-infrared (NIR) region.

In this study, we have developed an NIR interference spectrometer optimized for the observation of the HeI 2^3S–2^3P transition (1083 nm). Helium is an intrinsic element in fusion-related plasmas, and for the observation of the Zeeman splitting, helium atoms have an advantage that we can neglect the heating of atoms through molecular dissociation and that we can expect smaller Doppler broadening than for hydrogen atoms.[14] The spectrometer consists of a tunable Fabry-Perot etalon by which we can obtain a wavelength resolution of 15.1 pm and detect typical atomic temperature of a few thousand K in the SOL[10,11,14] as well as details of the change in the spectral line shape caused by the Zeeman splitting. For a long time, this type of spectrometer has been adopted for use with laboratory[15–17] and astrophysical[18–20] plasmas. It is particularly useful for infrared spectral lines, for which the achievement of high wavelength resolution is not easy with a grating spectrometer owing to the limitation in the number of grating grooves.

a)Author to whom correspondence should be addressed. Electronic mail: shikama@me.kyoto-u.ac.jp

II. NIR INTERFERENCE SPECTROMETER

A. Fabry-Perot etalon

A Fabry-Perot etalon[21–24] consists of two plane-parallel plates whose inner surfaces are coated with a highly reflective material. The wavelength at the peak transmittance of a light beam with the mth order of interference is given as

$$\lambda_m = \frac{2nl\cos\theta}{m}, \tag{1}$$

where n is the refractive index of the material filled in the gap between the plates, l is the gap length, and θ is the incident angle. We use a tunable etalon in which l is variable. For an ideal etalon, the transmittance profile is represented by an Airy function[22] or equivalently a Lorentzian function. The free spectral range (FSR), which is the wavelength spacing between adjacent transmission peaks, is expressed as

$$\Delta\lambda \simeq \frac{\lambda_m}{m}. \tag{2}$$

The full width at half maximum (FWHM) of the transmittance profile is expressed as

$$\delta\lambda_{\mathrm{R}} = \frac{\Delta\lambda}{N_{\mathrm{R}}}, \tag{3}$$

where $N_{\mathrm{R}} = \pi\sqrt{R}/(1-R)$ is the reflection finesse, and R is the reflectance of the inner surfaces.

The transmittance profile of an actual etalon has additional broadening caused by defects on the surfaces, i.e., curvature, tilt, and surface roughness, as well as the finite solid angle of the incident beam, and thus the profile deviates from the Airy function. Since the causes of the broadening are independent, the broadening can be approximated by[23,24]

$$\delta\lambda_{\mathrm{tot}}^2 = \delta\lambda_{\mathrm{R}}^2 + \delta\lambda_{\mathrm{D}}^2 + \delta\lambda_{\mathrm{A}}^2, \tag{4}$$

where $\delta\lambda_{\mathrm{tot}}$ is the total FWHM, and $\delta\lambda_{\mathrm{D}}$ and $\delta\lambda_{\mathrm{A}}$ are the FWHMs originating from the surface defects and finite solid angle associated with the incident beam, respectively. The effective finesse is then defined as

$$\frac{1}{N_{\mathrm{eff}}^2} = \left(\frac{\delta\lambda_{\mathrm{tot}}}{\Delta\lambda}\right)^2 = \frac{1}{N_{\mathrm{R}}^2} + \frac{1}{N_{\mathrm{D}}^2} + \frac{1}{N_{\mathrm{A}}^2}, \tag{5}$$

where $N_{\mathrm{D}} = \Delta\lambda/\delta\lambda_{\mathrm{D}}$ and $N_{\mathrm{A}} = \Delta\lambda/\delta\lambda_{\mathrm{A}}$ are the defect and aperture finesses, respectively. Note that N_{D} is approximately proportional to the wavelength, while N_{A} is constant as a function of the solid angle of the incident beam.

B. Specifications

A diagram of the spectrometer is shown in Fig. 1. Light is transferred via a quartz optical fiber (Mitsubishi Cable Industries ST50A-FV; core diameter 50 μm, cladding diameter 125 μm, NA 0.2), the sleeve of which is fixed by a four-axis mount (Tsukumo Engineering FC-22M), and the ejected light is collimated by an objective lens (Mitutoyo M Plan Apo NIR 10×, focal length 20 mm). The divergence of the collimated beam was adjusted to be smaller than 0.1° using a shearing interferometer[25] (Sigma koki SPV-05) by injecting 1060 nm light from a single-mode laser diode (Thorlabs L1060P200J), the temperature and injection current of which were controlled

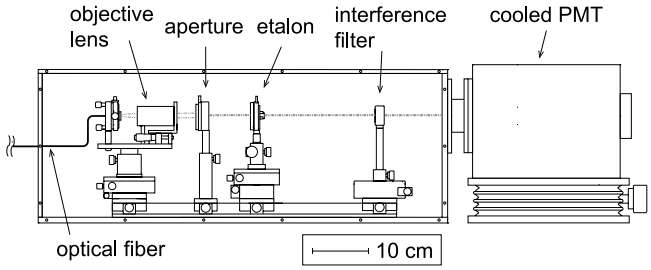

FIG. 1. Schematic diagram of the spectrometer.

by their respective drivers (Thorlabs TED200, LDC202). The obtained beam divergence results in a sufficiently large N_{A} in Eq. (5) for $\delta\lambda_{\mathrm{A}}$ to become negligibly small. The diameter of the collimated beam is about 8 mm, which is reduced with an additional aperture (Sigma koki IH-30). The resultant diameter affects two complementary quantities: the magnitude of N_{D} and the amount of light.

The beam is then injected into a tunable Fabry-Perot etalon (Light Machinery OP-1986-64; wavelength 1083 nm, air gap). The specifications of the etalon are $l = 982$ μm and $R \simeq 0.93$ at 1083 nm corresponding to $m \simeq 1800$, $\Delta\lambda \simeq 0.6$ nm, and $N_{\mathrm{R}} \simeq 43$. Note that the determination of the FSR involves a compromise between the available wavelength resolution and the observable wavelength range without mixing light transmitted through peaks with the next orders of interference; a FSR of 0.6 nm restricts us to observing the magnetic field effect with a field strength less than about 2.5 T. The gap length l is varied by applying a voltage to the piezoelectric element integrated in the etalon, where a frequency of up to 10 kHz is attainable for a variation corresponding to the FSR. For typical measurements, a low-frequency triangular voltage with 20 V_{pp}, which corresponds to about twice the FSR, and a frequency of 10 Hz was applied by a function generator (Agilent Technologies 33220A). The transmitted beam then passes through an interference filter (Omega Optical XB173-1080BP10; peak transmission wavelength 1080 nm, FWHM 10 nm) to exclude the other emission lines. Finally, the intensity of the beam is detected by a cooled photomultiplier tube (PMT) (Hamamatsu Photonics R5509-43; effective photocathode area 3×8 mm^2, cooled at −80 °C). The PMT current is converted into a voltage by a transimpedance amplifier, and the signal is recorded by a digitizer (National Instruments USB-4431; ±10 V, 24 bit, 102.4 kHz sampling). Considering the coupling between the beam and the etalon, we aligned the incidence of the beam to be normal to the etalon by minimizing the observed spectral line width of the 1060 nm laser light, since oblique incidence of the beam increases $\delta\lambda_{\mathrm{tot}}$ owing to decreases in N_{R} and N_{D}.

All the optical components are enclosed in a housing made of aluminum with a black alumite coating on the surface to minimize temperature fluctuations and to reduce stray light. In a laboratory with a typical air-conditioning system, we confirmed reproducibility of a measured spectrum over a period of several hours.

C. Wavelength calibration and determination of instrumental function

The voltage applied to the etalon was converted into a wavelength using a helium spectral line measured in a

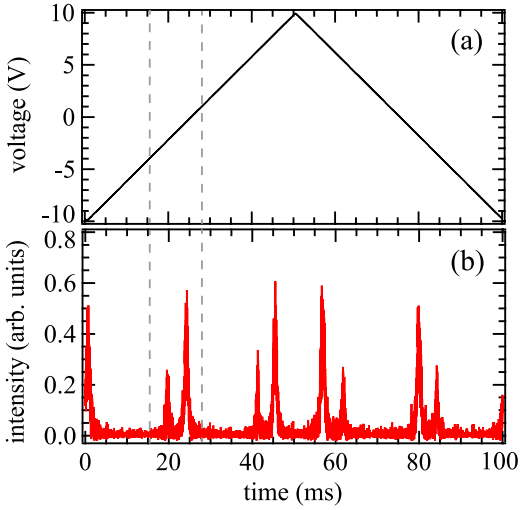

FIG. 2. Temporal evolutions of (a) voltage applied to the etalon and (b) intensity detected in a single period.

commercial discharge tube (Electro-Technic Products Spectrum Tube). The tube is made of glass and has an inner diameter of about 3 mm and a length of 260 mm, and the inside is filled with pure helium at a pressure of 20 Pa. It was operated with a dc current of 3 mA, and the emission was directly collected by the optical fiber at the center of the tube in a direction perpendicular to the longitudinal axis. The entire cross section of the tube was observed simultaneously through the aperture of the optical fiber. We set the diameter of the aperture in the spectrometer at 1 mm.

The temporal evolutions of the voltage and detected intensity in a single-period are shown in Figs. 2(a) and 2(b), respectively. We obtained the spectrum used for analysis after averaging data for 100 periods and reducing points within an interval of 40 mV into their average. Since displacement of the piezoelectric element has slight hysteresis, only spectra measured in the extending phase of the etalon were used.

The open circles in Fig. 3 show a measured spectrum, which is composed of the data between the vertical dashed lines in Fig. 2. From the evaluated voltages at the two observed peaks, the voltage was converted into the wavelength assuming linearity between the voltage and the etalon gap length. We evaluated the wavelengths at the two peaks assuming no Doppler shift and taking into account the effect of radiation reabsorption,[26] which results in variation of the relative intensities among the fine-structure transitions and thus slight shifts in the peak wavelengths. Although the effect of radiation reabsorption depends on the spatial distributions of the upper and lower state population densities and the emission and absorption line profiles, we estimated that the uncertainty in the evaluated peak wavelengths is smaller than 0.1 pm under plausible assumptions for these parameters and we thus neglected it. The conversion coefficient and its standard deviation, which originates from the uncertainty in the determination of the voltages at the two peaks and that in the linear fitting between the voltage and the wavelength, were estimated to be 67.4 ± 0.1 pm/V.

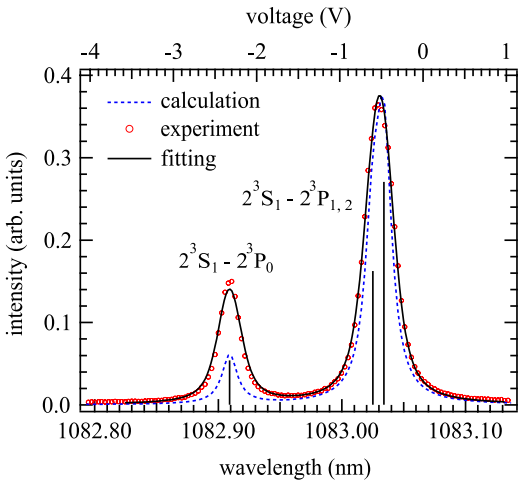

FIG. 3. HeI 2^3S–2^3P transition spectral line shapes. The open circles are measurements in a commercial glow discharge tube and the solid line is the fitting result. The dashed and vertical lines are the results of calculations with a Lorentzian width of 15.1 pm and without the effect of radiation reabsorption.

The instrumental function of the spectrometer was then measured using the above-mentioned 1060 nm laser light whose spectral line broadening is negligible compared with that of the transmittance profile of the etalon. The observed spectrum shown in Fig. 4 is fitted with the Lorentzian function, and the FWHM was found to be 219 ± 3 mV. We converted the evaluated voltage into a wavelength by modifying the conversion coefficient estimated at 1083 nm to the value at 1060 nm. By assuming the proportionality of $\mathrm{d}l$ and $\mathrm{d}V$, we can evaluate $\mathrm{d}\lambda_m/\mathrm{d}V$ at 1060 nm using the relation

$$\left.\frac{\mathrm{d}\lambda_m}{\mathrm{d}V}\right|_{1060\ \mathrm{nm}} = \left(\frac{1060}{1083}\right)\left.\frac{\mathrm{d}\lambda_m}{\mathrm{d}V}\right|_{1083\ \mathrm{nm}}, \tag{6}$$

where V is the applied voltage. From this relation, we determined the conversion coefficient and the FWHM of the instrumental function at 1060 nm to be 66.0 ± 0.1 pm/V and 14.5 ± 0.2 pm, respectively. The corresponding effective finesse is $N_{\mathrm{eff}} \simeq 39$. We can neglect the variation of N_{R} within 1060–1083 nm, which leads to $N_{\mathrm{R}} \simeq 43$ and $N_{\mathrm{D}} \simeq 93$. From these values, we can confirm that N_{eff} is dominated by N_{R}. On the basis of this fact, we concluded that $\delta\lambda_{\mathrm{tot}}$ is approximately proportional to the square of the wavelength, since $\delta\lambda_{\mathrm{R}}$ is proportional to λ_m^2 as can be seen from Eqs. (1)–(3) and we estimated the FWHM at 1083 nm to be 15.1 ± 0.2 pm.

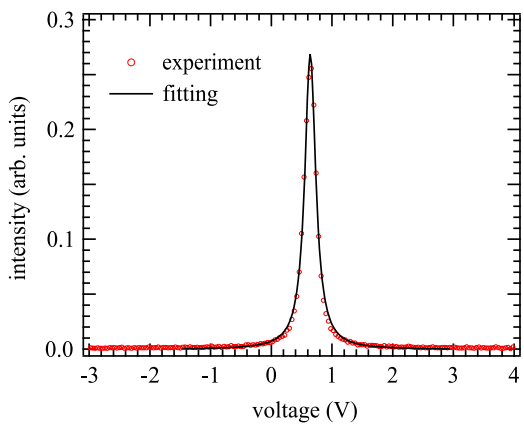

FIG. 4. Spectrum of 1060 nm single-mode laser diode.

The fitting curve to the helium spectral line is shown in Fig. 3 as a solid line. The curve consists of three Voigt functions whose Lorentzian width is fixed at the instrumental width of 15.1 pm, since the Stark broadening and pressure broadening are negligible.[26] Taking into account the propagation of the error contained in the instrumental width, the maximum, center, and minimum values of the evaluated Gaussian width are 14.3, 13.7, and 13.2 pm, respectively, and these widths are equivalent to atomic temperatures of 1360, 1250, and 1160 K, respectively. The error in the determined atomic temperature is thus approximately ±100 K. The dashed line in Fig. 3 shows the calculated spectral line shape with a Lorentzian width of 15.1 mm and no Doppler broadening when there is no effect of radiation reabsorption. The vertical lines indicate the relative emission intensities of the fine-structure transitions.

Regarding the error in the evaluation of the Doppler shift, if the S/N ratio of the spectrum is as large as that for Fig. 3, the standard deviation of the wavelength shift is estimated to be 0.2 pm. This corresponds to a velocity of about 60 m/s.

III. APPLICABILITY TO TORUS DEVICES

A. Calculation of spectral line shapes in LHD and QUEST

We investigate applicability of the present technique to actual torus devices by calculating the spectral line shapes expected to be observed in two torus devices currently under operation in Japan, LHD[27] and QUEST (Q-shu University Experiment with Steady State Spherical Tokamak).[28] In the calculation, we evaluated the Zeeman effect using first-order perturbation theory for degenerate levels.[29] For simplicity, we adopted a radial viewing chord on the mid-plane and assumed the following: emissions at the inboard and outboard SOLs are radially localized and have the same intensity, the magnetic field and the viewing chord are orthogonal, the atomic temperature is 2000 K, the atomic velocity is 1 km/s along the viewing chord toward the core region, the instrumental function is the Lorentzian function with a FWHM of 15.1 pm, and the effect of radiation reabsorption is neglected. The assumed values for the temperature and velocity are based on a result obtained in the TRIAM-1M tokamak.[14] The parameters used for the calculation are summarized in Table I.

Figures 5(a) and 5(b) show the calculated spectral line shapes for LHD and QUEST, respectively. For the spectrum of LHD, the magnetic field effect is conspicuous, and the two spectral lines originating from the inboard and outboard SOLs can be separated by analyzing the wavelengths and relative intensities of the small peaks appearing in the superposed spectrum. Even in a device with a smaller magnetic field strength such as QUEST, the magnetic field effect is observable. In particular, by analyzing the spectral line shape in the short-wavelength shoulder at 1082.8–1083.0 nm, the two superposed spectral lines can in principle be separated. Moreover, with the aid of polarization resolved spectroscopy,[10,11] separation of the superposed spectral lines becomes easier as can be seen in Fig. 5(c), which shows the σ-components of the spectrum in Fig. 5(b).

TABLE I. Parameters assumed for the calculation of the spectral line shapes in LHD and QUEST. The instrumental function is assumed to be a Lorentzian function with a FWHM of 15.1 pm.

Name of device	LHD	QUEST
Major radius (m)	3.6	0.68
Minor radius (m)	0.6	0.4
Magnetic field strength on axis (T)	2.75	0.25
Magnetic field strengthens in SOLs (T)	1.99, 1.51	0.61, 0.16
Atomic temperature (K)	2000	2000
Atomic velocity (km/s)[a]	1	1

[a]The flow velocity is value along the viewing chord, and the flow is assumed to be directed toward the core region.

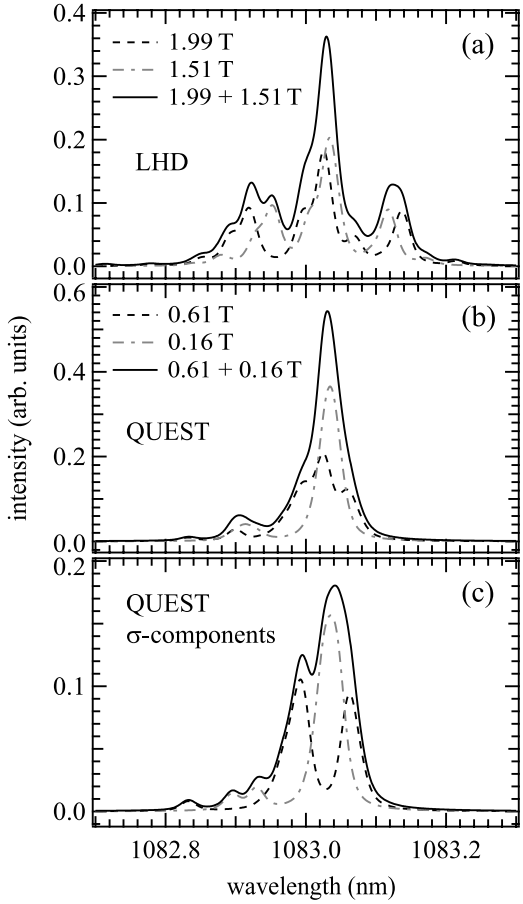

FIG. 5. Calculated spectral line shapes expected to be observed in (a) LHD and (b) QUEST. (c) σ-components of (b).

B. Experimental confirmation of magnetic field effect on spectral line shape

To confirm the validity of the calculated magnetic field effect on the spectral line shape, we compared the calculated spectral line shape with that measured in a glow discharge plasma under a uniform external magnetic field. We used a glow discharge tube made of glass with an inner diameter of 5 mm and a length of 190 mm and installed the tube in the bore of a cryogen-free superconducting magnet (Cryogenic 1721)[30] with its axis aligned parallel to the field direction. The inside of the tube was filled with pure helium at a pressure of 501 Pa. The tube was operated with a dc of 3 mA,

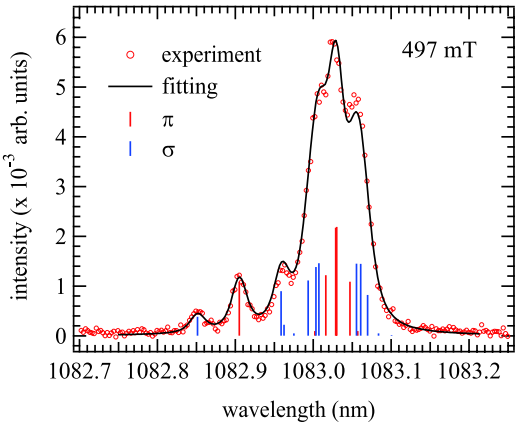

FIG. 6. Helium spectrum measured in a dc-glow discharge plasma under a magnetic field strength of 497 mT.

and the emission was collected in the same way as for the previously used commercial discharge tube. Regarding the magnetic field, the error in the field strength is less than 0.1 mT, and the inhomogeneity of the field at the center of the tube is less than 0.25% over a 10-mm-diameter sphere, which is larger than the observation volume. Since the emission intensity is smaller than that of the commercial discharge tube, data for 500 periods were averaged to obtain a sufficiently large S/N ratio and the instrumental function was set to 17.5 ± 0.2 pm.

Figure 6 shows the measured spectrum when the field strength was 497 mT, which is close to the value at the outboard SOL of QUEST in Fig. 5(b). We performed least-squares fitting of calculated spectral line shape, which includes radiation reabsorption,[31] to the experimentally obtained line shape. In the calculation, we assumed that the radial distributions of the 2^3P and 2^3S state population densities can be represented by the zeroth-order Bessel function and that the emission and absorption line profiles are spatially uniform and can be represented by a Gaussian function corresponding to the Doppler broadening. The fitting curve is shown as a solid line in the figure. From the fitting result, the field strength and temperature were estimated to be 489 ± 1 mT and 970 ± 90 K, respectively. We also measured spectra under field strengths of 446 and 396 mT, and the estimated field strengths were 436 ± 1 and 394 $^{+1}_{0}$ mT, respectively. In all the conditions, the measured line shapes are well reproduced by the calculation, and the deviations between the given and estimated field strengths are less than 3%.

IV. SUMMARY

We have developed a near-infrared interference spectrometer for measurements of the spatially resolved HeI 2^3S–2^3P transition spectral line shapes in magnetically confined torus plasmas. The spectrometer utilizes a tunable Fabry-Perot etalon, and a wavelength resolution of 15.1 pm was achieved. To confirm the applicability of the present technique to actual torus devices, we have calculated the spectral line shapes expected to be observed in LHD and QUEST and we found that the spectral lines which originate from the inboard and outboard SOLs can in principle be separated by using the difference in the Zeeman splitting.

ACKNOWLEDGMENTS

This work was supported in part by a Kurata Grant from Kurata Memorial Hitachi Science and Technology Foundation, a NIFS Collaborative Research Program (No. NIFS14KUTR099), and a Collaborative Research Program of Research Institute for Applied Mechanics, Kyushu University (No. 26FP-19).

[1]N. Asakura and ITPA SOL and Divertor Topical Group, J. Nucl. Mater. **363-365**, 41 (2007).
[2]N. Smick, B. LaBombard, and I. H. Hutchinson, Nucl. Fusion **53**, 023001 (2013).
[3]A. Yu. Pigarov, S. I. Krasheninnikov, and B. LaBombard, Contrib. Plasma Phys. **46**, 604 (2006).
[4]H. Bufferand, G. Ciraolo, G. Dif-Pradalier, P. Ghendrih, Ph. Tamain, Y. Marandet, and E. Serre, Plasma Phys. Controlled Fusion **56**, 122001 (2014).
[5]B. L. Welch, J. L. Weaver, H. R. Griem, W. A. Noonan, J. Terry, B. Lipschultz, and C. S. Pitcher, Phys. Plasmas **8**, 1253 (2001).
[6]V. Kotov, D. Reiter, A. S. Kukushkin, H. D. Pacher, P. Börner, and S. Wiesen, Contrib. Plasma Phys. **46**, 635 (2006).
[7]J. Rosato, D. Reiter, H. Capes, S. Ferri, L. Godbert-Mouret, M. Koubiti, Y. Marandet, and R. Stamm, J. Nucl. Mater. **390-391**, 1106 (2009).
[8]P. G. Carolan, M. J. Forrest, N. J. Peacock, and D. L. Trotman, Plasma Phys. Controlled Fusion **27**, 1101 (1985).
[9]J. L. Weaver, B. L. Welch, H. R. Griem, J. Terry, B. Lipschultz, C. S. Pitcher, S. Wolfe, D. A. Pappas, and C. Boswell, Rev. Sci. Instrum. **71**, 1664 (2000).
[10]T. Shikama, K. Fujii, S. Kado, H. Zushi, M. Sakamoto, A. Iwamae, M. Goto, S. Morita, and M. Hasuo, Can. J. Phys. **89**, 495 (2011), and references therein.
[11]K. Mizushiri, K. Fujii, T. Shikama, A. Iwamae, M. Goto, S. Morita, and M. Hasuo, Plasma Phys. Controlled Fusion **53**, 105012 (2011).
[12]R. Bhattacharyay, H. Zushi, K. Nakamura, T. Shikama, M. Sakamoto, N. Yoshida, S. Kado, K. Sawada, Y. Hirooka, K. Nakamura *et al.*, Nucl. Fusion **47**, 864 (2007).
[13]G. Arnoux, S. Devaux, D. Alves, I. Balboa, C. Balorin, N. Balshaw, M. Beldishevski, P. Carvalho, M. Clever, S. Cramp *et al.*, Rev. Sci. Instrum. **83**, 10D727 (2012).
[14]T. Shikama, S. Kado, H. Zushi, M. Sakamoto, A. Iwamae, and S. Tanaka, Plasma Phys. Controlled Fusion **48**, 1125 (2006).
[15]J. R. Creig and J. Cooper, Appl. Opt. **7**, 2166 (1968), and references therein.
[16]C. H. Skinner, H. Adler, R. V. Budny, J. H. Kamperschroer, L. C. Johnson, A. T. Ramsey, and D. P. Stotler, Nucl. Fusion **35**, 143 (1995).
[17]S. Löhle and S. Lein, Rev. Sci. Instrum. **83**, 053111 (2012).
[18]J. E. Geake, J. Ring, and N. J. Woolf, Mon. Not. R. Astron. Soc. **119**, 616 (1959).
[19]J. Meaburn, Astrophys. Space Sci. **9**, 206 (1970).
[20]P. D. Atherton, K. Taylor, C. D. Pike, C. F. W. Harme, N. M. Parker, and R. N. Hook, Mon. Not. R. Astron. Soc. **201**, 661 (1982).
[21]J. F. Mulligan, Am. J. Phys. **66**, 797 (1998).
[22]E. Hecht, *Optics*, 4th ed. (Addison-Wesley, 2002), pp. 421–423.
[23]P. D. Atherton, N. K. Reay, J. Ring, and T. R. Hicks, Opt. Eng. **20**, 806 (1981).
[24]A. R. Martel and A. Fullerton, Space Telescope Science Institute Technical Report, 2011.
[25]M. E. Riley and M. A. Gusinow, Appl. Opt. **16**, 2753 (1977).
[26]T. Shikama, S. Ogane, H. Ishii, Y. Iida, and M. Hasuo, Jpn. J. Appl. Phys., Part 1 **53**, 086101 (2014).
[27]M. Goto and S. Morita, Phys. Rev. E **65**, 026401 (2002).
[28]K. Hanada, K. Sato, H. Zushi, K. Nakamura, M. Sakamoto, H. Idei, M. Hasegawa, Y. Takase, O. Mitarai, T. Maekawa *et al.*, Plasma Fusion Res. **5**, S1007 (2010).
[29]M. Goto, in *Plasma Polarization Spectroscopy*, edited by T. Fujimoto and A. Iwamae (Springer, 2007), Chap. 2.
[30]T. Shikama, N. Naka, and M. Hasuo, J. Quant. Spectrosc. Radiat. Transfer **113**, 294 (2012).
[31]T. Shikama, S. Ogane, Y. Iida, and M. Hasuo, "Measurement of the helium 2^3S metastable atom density by observation of the change in the 2^3S–2^3P emission line shape due to radiation reabsorption" (unpublished).